Geogy J. Abraham*, Rajan Bhambroo, V. Kain, G. K. Dey and V. S. Raja

Intergranular Corrosion Susceptibility of Alloy 600 after Autogenous Tungsten Inert Gas and Laser Beam Welding using Electrochemical Technique

Abstract: Intergranular corrosion and intergranular stress corrosion cracking is influenced by precipitation of chromium carbides at grain boundaries and formation of chromium depletion regions. The present study focuses on understanding the carbide precipitation and subsequent sensitization in the weldments of Alloy 600 using two different welding techniques. The effect of heat input on microstructure and IGC susceptibility was measured using electrochemical reactivation test. The SEM studies were done to evaluate the presence of chromium depleted regions. The carbide was indentified to be Cr_7C_3 using TEM. The laser beam weldments showed an increased resistance to IGC as compared to TIG weldments.

Keywords: Alloy 600, SEM, TEM, intergranular corrosion, welding

***Corresponding author: Geogy J. Abraham:** Materials Science Division, Bhabha Atomic Research Centre, Mumbai 400085, India
E-mail: gja@barc.gov.in
Rajan Bhambroo, V. S. Raja: Department of Metallurgical Engineering and Material Science, IIT Bombay, Mumbai 400076, India
V. Kain, G. K. Dey: Materials Science Division, Bhabha Atomic Research Centre, Mumbai 400085, India

1 Introduction

Chemical composition and microstructure of alloys play an important role in determining their resistance to localized corrosion such as intergranular corrosion (IGC) and intergranular stress corrosion cracking (IGSCC). Nickel base alloys and Alloy 600 in particular are highly susceptible to sensitization since they have 15–17 wt% chromium content and show low carbon solubility (~0.001 wt%) in the sensitization temperature regime of 500–800 °C [1]. Alloy 600 is being used as SG tubing material in older generation PWRs and is gradually being replaced by Alloy 690 which has higher chromium content and hence improved corrosion resistance [2]. Apart from SG tubing, Alloy 600 is also being used for control rod drive mechanism nozzle, thermocouple tubes, instrument nozzle etc. in nuclear power plants. The major degradation problems associated with Alloy 600 in nuclear reactors are IGSCC and IGC [3, 4]. There are several cases of cracking in reactors at service nozzle regions and these cracking are mostly concentrated in weld fusion zone (WFZ) and heat affected zone (HAZ) region of the weldments [5–9]. Steam generator (SG) layup, start up and shutdown transients are the most vulnerable conditions for SG tube failures from the secondary side. When there are both oxidizing conditions and acid forming impurities present (chloride and sulphate, for example) during these periods pitting and subsequent TGSCC occur on SG tubes [10, 11]. Thus, IGC and pitting corrosion are found to be initiating factors for TGSCC and IGSCC failures of nickel alloy steam generator tubes. IGSCC of stainless steels and nickel base alloys has been reported from both BWRs and PWRs. The alloy 600 is not typically used in PHWRs. The results obtained in this study would primarily be of importance for PWRs and for BWRs. There are published reports [13–16] that indicate that Alloy 600 steam generator tubes in PWRs are prone to IGSCC due to effects of chromium depletion and chromium carbides at grain boundaries. In this application, presence of discrete chromium carbides at grain boundaries is taken as beneficial against IGSCC. Also Kilian et al. [15] reported IGC from secondary side of steam generator tubes due to fabrication aspects in PWRs. There are published reports on Alloy 600 sensitization [16] being important in BWRs from IGSCC point of view. These reports clearly bring out the importance of sensitization in Alloy 600 in both PWRs and BWRs [12–16].

Grain boundary chemistry plays an important role in influencing IGC/IGSCC. Fabrication of nickel alloys involves welding, which is generally done by gas tungsten arc welding or tungsten inert gas (GTAW/TIG). Such welding processes generate high amount of heat within the weld fusion zone (WFZ) and heat affected zone (HAZ) of welded components leading to sensitization of weldments. Sensitization occurs at 500–800 °C when chromium carbides precipitate at the grain boundaries leaving

the adjacent area depleted of chromium below 12 wt%. Welding of Alloy 600 SG tubes result in sensitization along HAZ due to alloy chemistry and favorable temperature regime. Hence, a judicious choice of welding technique has to be made to keep in check the heat input given to the weldment and ensure faster cooling rates during welding. Welding not only alters the microstructure of base metal (e.g. by forming grain boundary carbides), but also introduces high levels of local strain immediately adjacent to the fusion line [17]. These changes may decrease the base metal's resistance to SCC initiation and propagation. In order to mitigate the problem of sensitization in weldments, laser beam welding (LBW) technique has been shown to be effective for stainless steels and nickel alloys [18, 19]. The advantage of this technique is that it employs lesser heat input and faster cooling rates which decrease the chromium carbide precipitation that generally forms in the HAZ region of the weldment [20, 21].

IGC occurs mainly due to sensitization [22, 23]. Techniques such as ASTM standard A 262 Practice A–F are used for evaluation of stainless steels (SS) for susceptibility to IGC [24]. Apart from A 262 Practice A test, all the other tests are destructive in nature. For nickel base alloys, ASTM G28 is used to evaluate susceptibility to IGC [25]. Since Alloy 600 is highly prone to IGC, G28 recommends short test duration of 24 h only. An alternative non-destructive electrochemical technique is the electrochemical potentiodynamic reactivation (EPR) technique for evaluating [26] degree of sensitization (DOS). The other technique to measure DOS value is in sulphuric acid and sodium chloride environment using the AC impedance technique at transpassive potential values above 1.05 V_{SCE} (saturated calomel electrode) which attacks the grain boundary [27].

The present study focuses on understanding the carbide precipitation and sensitization in weldments of Alloy 600 using two different welding techniques. The effect of heat input on microstructure by optical microscopy and IGC susceptibility is measured in terms of degree of sensitization (DOS) using double loop electrochemical potentiokinetic reactivation (DL-EPR) test. The microstructural characterization was carried out using scanning electron microscope (SEM) to understand the degree of attack after DL-EPR test along chromium depleted regions and transmission electron microscope (TEM) analysis was done to identify the type of carbides formed along grain boundaries.

Table 1: Chemical composition of Alloy 600 used in present study.

	Elements (wt%)						
Alloy	**Ni**	**Cr**	**Fe**	**C**	**Mn**	**Si**	**Ti**
600	71.2	17.03	8.71	0.06	0.8	0.10	0.35

2 Experimental details

2.1 Material and metallography

Alloy 600 used for the present study was obtained in the form of sheets of 2.5 mm thickness. These sheets were analyzed for chemical composition as per ASTM E1473 [28]. The composition of the alloy is given in Table 1. The as received specimens of 15 mm × 10 mm × 2.5 mm were encapsulated in a quartz tube with 0.02 bar (2000 Pa) pressure maintained using helium gas, and was subsequently given a solution annealing treatment at 1100 °C for 30 min and water quenched [29].

Microstructure studies on Alloy 600 were done by optical microscopy. Solution annealed (SA) Alloy 600 were etched by electrolytic etching using 10 wt% oxalic acid solution at a potential of 10 V for a period of 60 s. The carbides present in SA Alloy 600 were revealed by etching with Murakami's reagent (10 gm potassium hydroxide + 10 gm potassium ferricyanide in 100 ml water, swabbing for a few seconds).

2.2 TIG and Laser welding

2.2.1 Welding parameters

Autogenous welding of 2.5 mm thick SA plates was carried out using TIG and LB welding techniques, the details of which are described below. Briefly, an arc/laser beam was scanned over the length of the plate yielding through thickness melting which caused typical heat input of such welding operations and resulted in changes in microstructure. The TIG welding was performed in pure argon shielding gas using the following welding parameters: 130–135 A, 16–18 V and weld electrode speed of 80–90 mm min^{-1}. LB welding process was carried out using Nd-YAG laser with a mean power of 800 W, spot size of 600 μm, torch speed of 600 mm min^{-1} and a shielding gas (argon) pressure of 0.5 kg cm^{-2}.

In this study, the weldment region which melted and solidified is referred to as the (WFZ), the region adjacent to

the WFZ which has been affected by the heat input is referred to as the (HAZ) and the unaffected area of the weldment is referred to as base metal.

2.2.2 Microstructural characterization

Microstructural studies on Alloy 600 weldments were done by optical microscopy. Weldments were etched by electrolytic etching using 10% oxalic acid solution at a potential of 10 V for a period of 60 s The carbides present in the weldments were revealed by etching with Murakami's reagent (10 gm potassium hydroxide + 10 gm potassium ferricyanide in 100 ml water, swabbing for a few seconds). Scanning electron microscopy (SEM) analysis of the specimen after (DL-EPR) test was done for different regions of the weldment.

2.2.3 Ferrite measurements

Magnetic susceptibility of TIG welded and Laser-welded samples of Alloy 600 were measured using a portable ferrite meter. Individual regions of the weldment, i.e. base metal, HAZ and WFZ were examined. A range of ferrite number (FN) was obtained for each region of the weldments.

2.3 Electrochemical characterization

Electrochemical studies were carried out in a standard electrochemical cell with a three electrode set-up consisting of a saturated calomel electrode (SCE) as reference electrode, platinum as counter electrode and Alloy 600 specimen as working electrode. A potentiostat was used to carry out electrochemical measurements. The specimens were mounted in a cold setting resin with an approximate area of 1 cm^2 with precautions taken to avoid any crevice formation at the specimen/mount interface. The specimen were ground on silicon carbide papers and finally polished with a diamond paste of 1 µm size. DOS value for welded Alloy 600 was evaluated by the (DL-EPR) test in 0.01 M H_2SO_4 and 2×10^{-4} M KSCN (deaerated) at room temperature with a scanning rate of 0.5 mV s^{-1} [30]. The test solution was continuously purged with high purity argon gas before and during the experiment. The specimen potentials were scanned from open circuit potential (OCP) to +500 mV_{SCE} and then back to OCP. The ratio of reactivation current (I_r) and activation current (I_a) multiplied by 100 is taken as the DOS which is a measure of the susceptibility to IGC. The different regions of interest in the weldment were studied by masking the remaining areas by lacquer. The average value of DOS from three experiments carried out for each condition has been reported.

2.4 Transmission electron microscopy

The 2.5 mm thick strips of sensitized Alloy 600 (700 °C/16 h) were thinned down to about 120 µm thickness by polishing on SiC papers. After this, they were ultrasonically cleaned with soap solution and acetone and discs of 3 mm diameter were punched out. The electron transparent specimens were prepared from this thin foil by twin-jet electropolishing at a voltage of 30 V in a solution of methanol and perchloric acid (9:1 ratio) maintained at –30 to –35 °C. Specimens were examined using TEM at 160 kV.

3 Results and discussion

3.1 Microstructural characterization

Base metal specimen showed "ditch" structure (i.e. at least one grain completely surrounded by chromium carbides/chromium depletion regions when viewed at 100×) even in SA condition due to grain boundary carbide precipitation as seen in Fig. 1. The carbide precipitation is a result of the low solubility of carbon in nickel alloys making it difficult to suppress carbide precipitation as it passes through the sensitization temperature range of 500–800 °C during quenching [1].

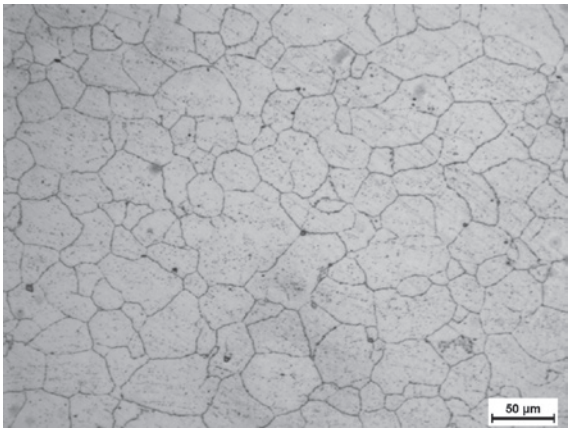

Fig. 1: Optical micrograph of solution annealed Alloy 600 (1100 °C/30 min) after ASTM A262 Practice A test showing the attack along grain boundaries.

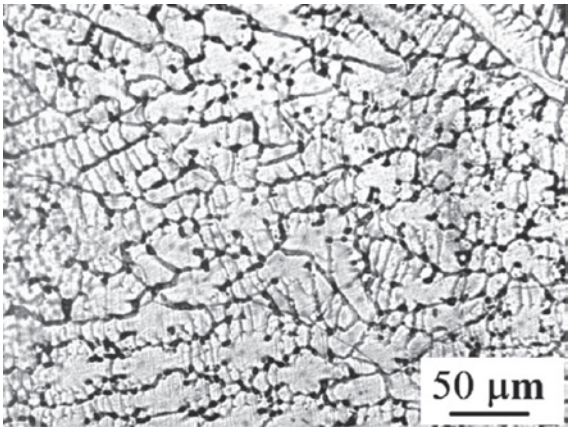

(a)

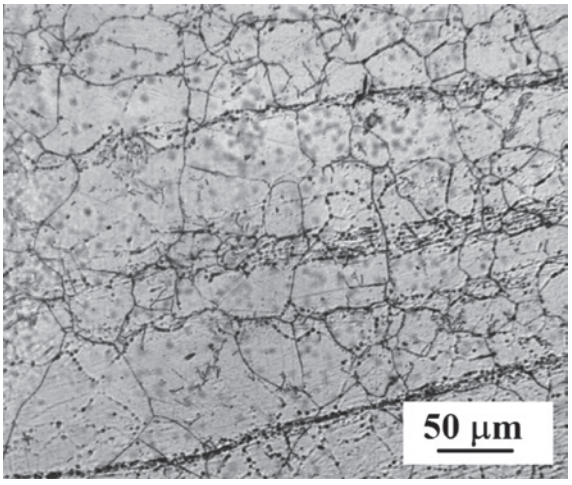

(b)

Fig. 2: Optical micrographs of (a) WFZ and (b) HAZ of Alloy 600 TIG weldments showing the attack at grain boundaries and along the flow lines after ASTM A262 Practice A test.

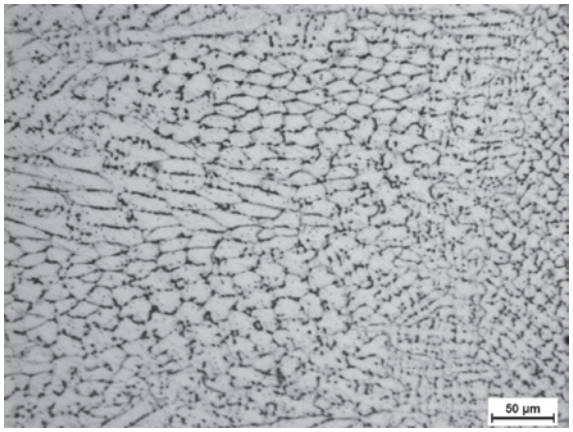

(a)

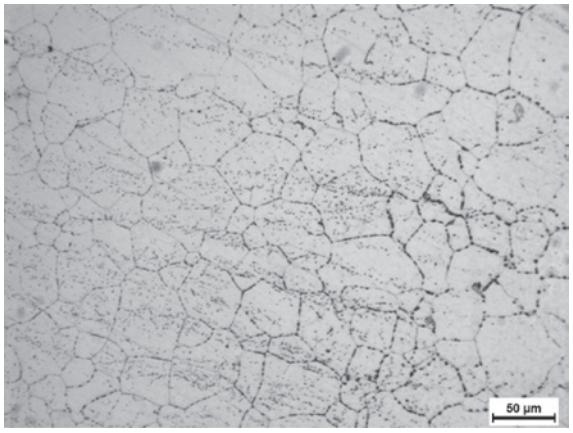

(b)

Fig. 3: Optical micrographs of (a) WFZ and (b) HAZ of Alloy 600 LB weldments after ASTM A262 Practice A test showing attack along the grain boundaries and within the grain.

TIG welding resulted in microstructural changes which rendered certain regions of the weldment i.e. HAZ more prone to localized corrosion attack. Alloy 600 welded using the TIG welding technique showed the WFZ of width 6 mm and HAZ of width 2 mm. The high heat input resulted in increased kinetics and growth of carbide precipitates in the WFZ and HAZ as shown in Fig. 2(a) and (b).

LB welding resulted in narrow WFZ (2 mm) width and HAZ (0.7 mm). This decrease in zone widths resulted due to low heat input from LB welding where the welding power density is approximated to be 10^4–10^5 W/mm^2 [17]. The heat input calculated for LB welding technique based on the heat input equations given by Fuerschbach [31, 32] was 68 J/mm which was considerably lower than that in TIG welding with 1147 J/mm. This resulted in lesser carbide precipitation in the weldments and a more finely spaced dendrites in the WFZ as shown in Fig. 3(a) and (b).

The carbides in SA samples is quite small in size as seen in Fig. 4(a) after etching by Murakami's reagent that revealed the carbides present in Alloy 600. There is increase in size of the carbides as shown in Fig. 4(b) and (c) for WFZ and HAZ of TIG weldment of Alloy 600 respectively. The size of the carbides present in the WFZ is larger (around 1.6 µm) than the ones present in the HAZ region (500–700 nm). The reported M_7C_3 carbide size for Alloy 600 in as cast structure is around 1.0–1.5 µm [33]. The increased size of carbides as compared to the SA and decreased carbide size than TIG welded samples are shown in Fig. 4(d) and (e) for Alloy 600 LB weldments. The heat input and cooling rate of a welding technique would indirectly affect carbide precipitation and the carbide size which is observed in the optical micrographs Fig. 4(b)–(e).

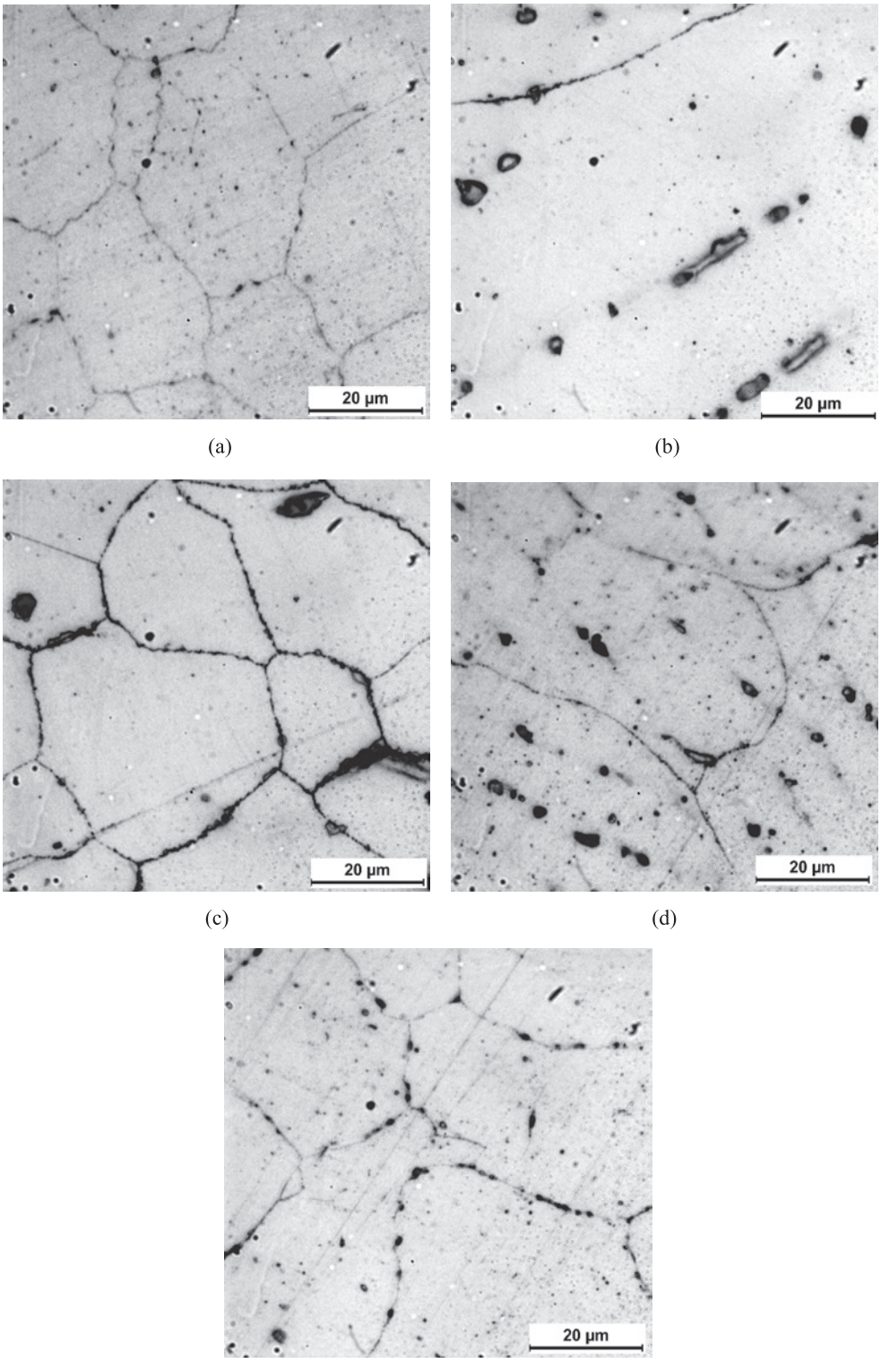

Fig. 4: Optical micrographs of (a) solution annealed, (b) WFZ of TIG weldment, (c) HAZ of TIG weldment, (d) WFZ of LB weldment, and (e) HAZ of LB weldment after etching with Murakami's reagent to reveal the carbides.

3.2 Magnetic susceptibility

The ferritemeter readings showed ferrite number (FN) of Alloy 600 in TIG and LB welded conditions and are listed in Table 2. However, orientation imaging microscopy (OIM) and X-ray diffraction (XRD) measurements of Alloy 600 weldments showed the presence of only austenite phase which is paramagnetic in nature [34]. The presence of ferrite number shown by the ferrite meter is interpreted in the following manner. The magnetic behavior indicated as FN may be attributed to chromium depletion. Chromium depletion at certain regions due to carbide formation makes high nickel alloys ferromagnetic (from paramagnetic in non-sensitized condition) [35]. Earlier work reported, that for Alloy 800, the Curie temperature shifted to higher values for the sensitized condition from 20 °C in the annealed condition due to chromium depletion around chromium carbides [36]. Kowaka et al. [37] showed that in Alloy 600, the increased magnetic susceptibility for sensitized condition was reflected by shift in Curie temperatures below 250 °C. Therefore, the magnetic susceptibility in the welded condition for the TIG weldments is attributed to formation of chromium depletion around the precipitated carbides. The measured ferrite meter readings in the weldments are quite low and are reflective of the very narrow width of chromium depletion regions that get developed in Alloy 600 upon sensitization [14].

Table 2: Ferrite meter readings showing magnetic susceptibility in Alloy 600 weldments.

Alloy 600	Base (FN)	HAZ (FN)	WFZ (FN)
TIG	0.17–0.30	0.29–0.56	0.63–0.81
LB	0.15–0.28	0.21–0.52	0.41–0.61

3.3 Reactivation behaviour of Alloy 600 TIG weldments

The DL-EPR plots of Alloy 600 TIG weldment showed (Fig. 5) similar anodic current peaks in the forward direction (I_a) for all the three regions of the weldment. However, for the reactivation peak (I_r) the WFZ showed highest current followed by the HAZ and the base metal. Base metal in solution annealed condition (1100 °C/30 min) also showed sufficient reactivation current indicating attack due to presence of chromium depletion regions. Examination of this specimen after the completion of DL-EPR test under

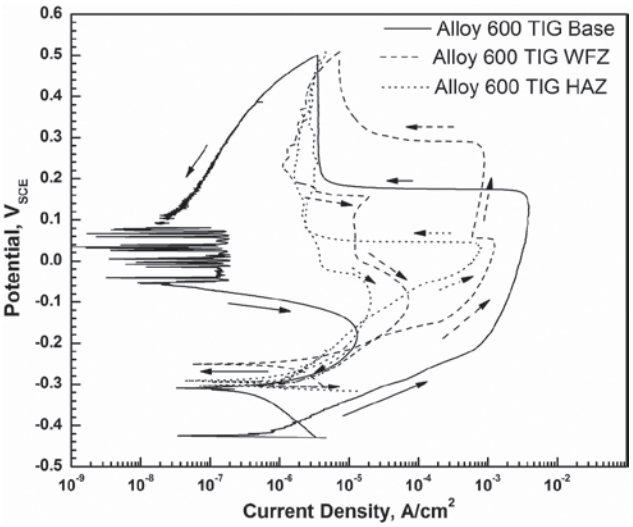

Fig. 5: DL-EPR plots for TIG welded Alloy 600 in 0.01 M H_2SO_4 + 20 ppm KSCN (deaerated) at RT.

SEM showed (Fig. 6(a)) attack along the grain boundary but the attack was discontinuous in nature. Chromium depletion due to intragranular carbide precipitation at a few locations was also observed. The higher carbon content in Alloy 600 combined with inherently poor solubility of carbon in nickel base alloys are the main causes for this sensitization, since they shift the critical cooling rate required to avoid sensitization to a higher value and the water quenching step is not fast enough to avoid the precipitation process. The commercially available nickel base Alloy 600 as per commonly followed guidelines shows a maximum of 0.15 wt% carbon content [29]. The carbon that we have in Alloy 600 is 0.06 wt% C that is within the specified limit of this alloy. The use of a high carbon Alloy 600 would enable us to clearly differentiate the effect of heat input on its IGC susceptibility. Alloy 600 used by other researchers to study IGC behaviour also had similar carbon contents as that used in the present study [38–40]. Lesser chromium content, i.e. only 17 wt% in Alloy 600 as compared to Alloy 690 also resulted in the chromium levels going down to lower values and hence higher DOS values shown in the EPR test [16]. The HAZ showed a comparatively low DOS value and SEM examination of the surfaces showed (Fig. 6(b)) the presence of a chromium depletion having a larger width of attacked regions around certain grain boundaries and also the presence of numerous intragranular chromium depletion locations which are discrete in nature. The WFZ showed the highest DOS value among all the three regions. Grain boundary attack is clearly visible from SEM micrograph for the WFZ (Fig. 6(c)).

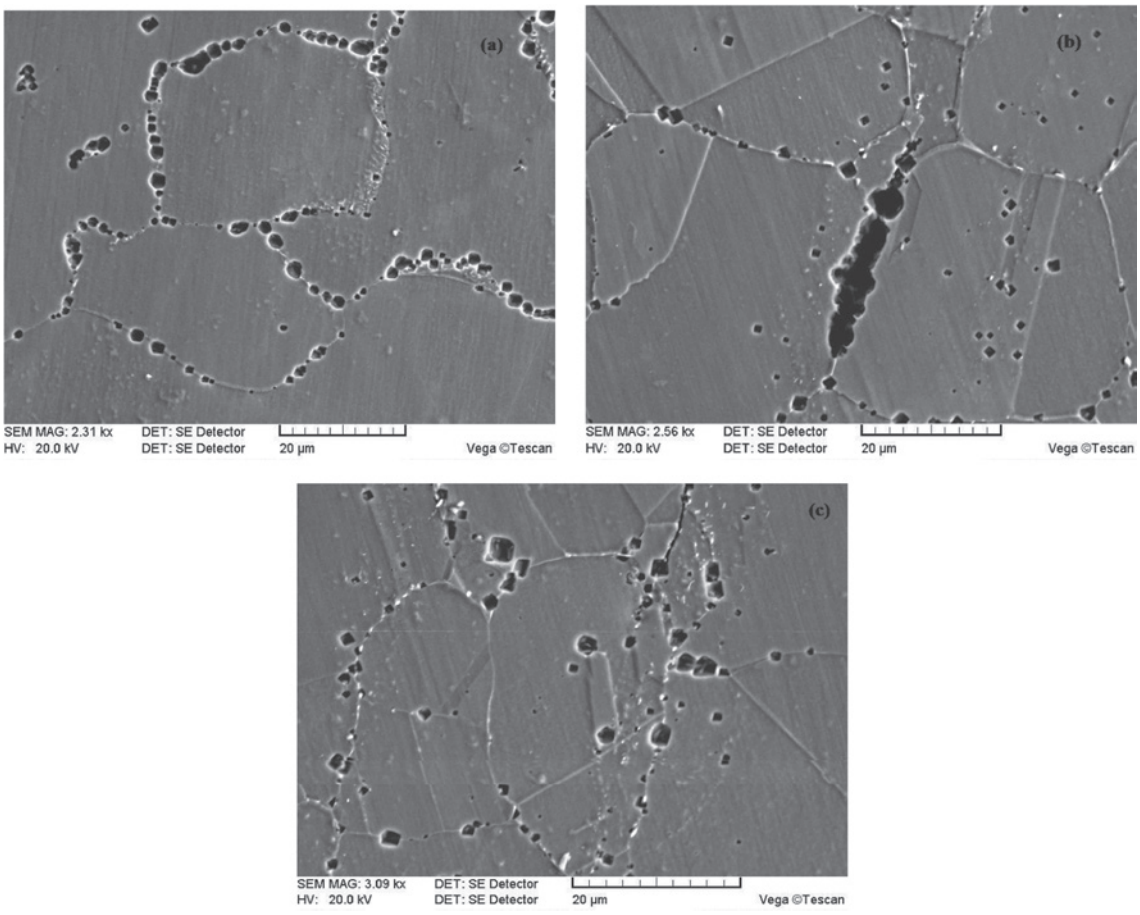

Fig. 6: SEM micrograph of Alloy 600 TIG weldment after DL-EPR exposure in 0.01 M H_2SO_4 + 20 ppm KSCN (deaerated) at RT (a) base metal, (b) HAZ, and (c) WFZ showing the attack along the grain boundaries with chromium depletion.

3.4 Reactivation behaviour of Alloy 600 LB weldments

DL-EPR plots for laser welded Alloy 600 showed (Fig. 7) decreased current values for activation and reactivation conditions as compared to the corresponding zones of TIG welded specimen. The HAZ of LB welded specimen showed a high DOS value. The SEM micrograph of DL-EPR tested HAZ showed discrete attack at grain boundaries (Fig. 8(a)). The WFZ in laser welded condition showed similar behavior as that of TIG welded sample. SEM examination showed (Fig. 8(b)) that there is discontinuous attack in the WFZ, mainly observed along dendrites with some attack at inter dendritic regions.

The increased DOS values for the TIG weldments can be attributed to the increased carbide precipitation in TIG weldments. Alloy 600 in the TIG and LB welded conditions showed the maximum DOS value for WFZ. During welding there is a probability of formation of M_7C_3 and $M_{23}C_6$ carbides in Alloy 600 and it results in the formation

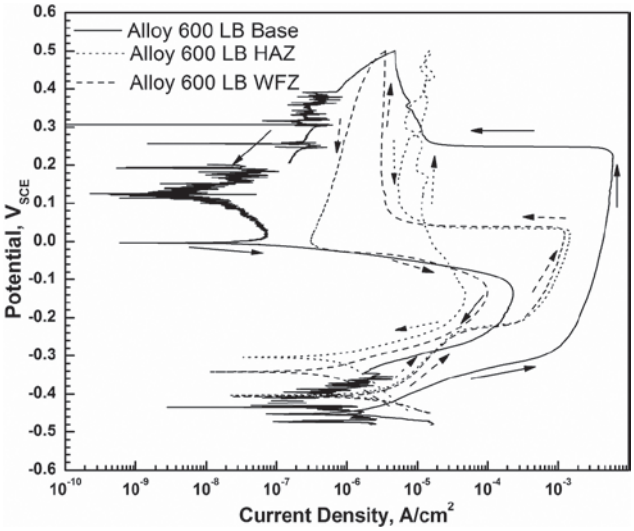

Fig. 7: DL-EPR plots for LB welded Alloy 600 in 0.01 M H_2SO_4 + 20 ppm KSCN (deaerated) at RT.

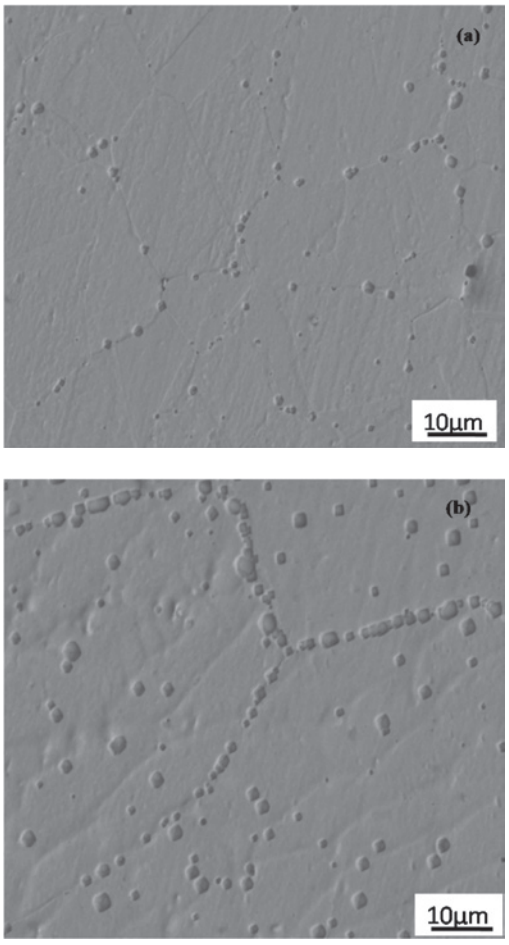

Fig. 8: SEM micrograph of Alloy 600 LB weldment after DL-EPR exposure in 0.01 M H_2SO_4 + 20 ppm KSCN (deaerated) at RT (a) HAZ and (b) WFZ showing increased presence of carbide in the WFZ as compared to HAZ.

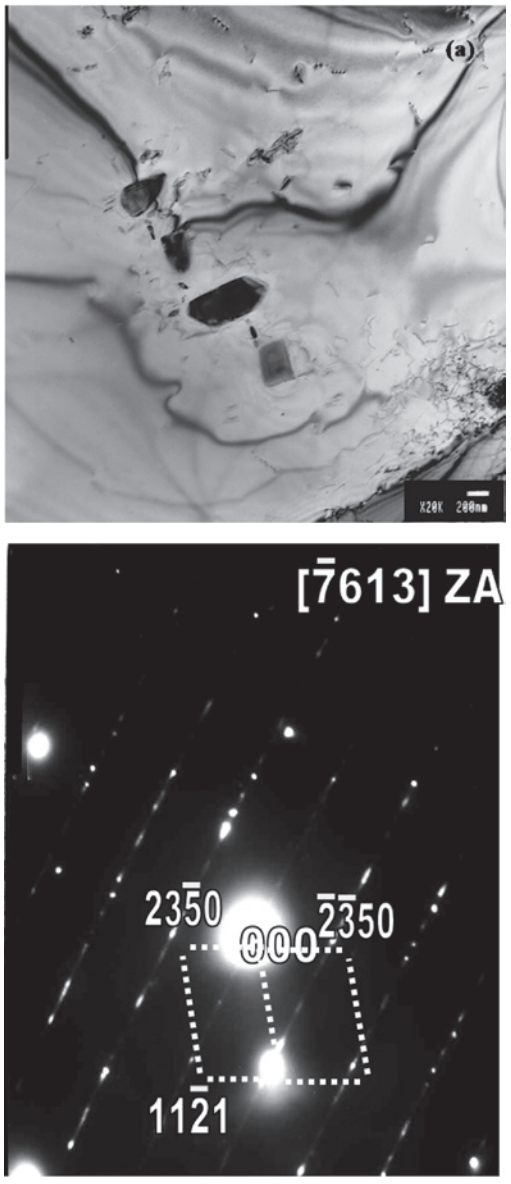

Fig. 9: (a) TEM micrograph of carbides in Alloy 600 (700 °C/16 h) and (b) diffraction pattern of the Cr_7C_3 carbide.

of excessive chromium depletion. The chromium levels fall to low values especially because the chromium content in the alloy is 17 wt% and carbon level is 0.06 wt%. Was et al. [41] found, from Huey and Streicher tests, that severe IGC occurred when the measured Cr concentration on the grain boundary was below 9 wt% with a nearly continuous distribution of grain boundary Cr-rich carbides. The TEM analysis carried out for the sensitized Alloy 600 showed the grain boundaries were decorated with discrete Cr_7C_3 carbides (Fig. 9). These Cr_7C_3 carbides are shown to have lesser chromium content in the matrix in equilibrium with the carbide as compared to $Cr_{23}C_6$ [41]. The formation of Cr_7C_3 therefore resulted in increased chromium depletion along the grain boundaries resulting in higher DOS values.

The carbide precipitation also depends on the various factors such as carbon content, temperature-time combination and the grain boundary characteristics [42]. Scarberry et al. [43] have shown that for a given solution-annealing temperature, samples with lower carbon contents have much slower carbide precipitation and sensitization kinetics upon ageing. Alloy 600 taken for the present study (Table 1) showed a 0.06 wt% carbon content which resulted in heavy carbide precipitation even in the WFZ along dendrites. The pre-existing carbides grow in size and new carbides get formed upon subjecting the alloy to heat since the available free carbon in the matrix is quite high. The DOS values calculated showed that LB welded samples have one order lower values as compared to TIG welded samples primarily due to low heat input during LB welding.

3.5 Comparison of TIG and LB welding on IGC

The microstructure obtained after the ASTM A262 Practice A test for the SA material showed a "ditch" structure (Fig. 1). The Practice A test which is an oxalic acid etch test is carried out at a potential regime corresponding to transpassive potential. At this high transpassive potential, the dissolution of the carbide as well as the chromium depleted region takes place resulting in a wide region of attack as seen in the optical micrographs (Figs. 1–3). Fig. 2(b) and Fig. 3(b) do indicate banded structure. However, these microstructures are after a strong electro etching test in oxalic acid (practice A, A262, ASTM). These do tend to show in homogeneity in the material. After the EPR test (Figs. 6 and 8) did not reveal any banding in the structure. This indicated that the in homogeneity in the material did not affect electrochemical activity hence not affected the EPR tests.

However, the microstructure after the DL-EPR exposure showed a "dual" structure (indicating some ditching at grain boundaries, but no grain completely encircled by attack/dissolution at chromium carbides/depletion regions) (Fig. 6(a)). In the DL-EPR test, the region attacked in the microstructure is only those that have a chromium depletion less than 12 wt% and there is no attack at the chromium carbides. The regions showing chromium above 12 wt% are shown as not attacked [17–19]. Hence, the SEM micrographs after DL-EPR test, in case of TIG and LBW, showed discrete attack along grain boundaries and also within grains. This brings out the prowess of the DL-EPR test to give an accurate estimate of the chromium depletion and hence the sensitization behavior of the microstructure as compared to oxalic acid etch test. The oxalic acid test would overestimate the IGC susceptibility. Thus materials that may seem to have a ditch structure during the ASTM A262 Practice A test can turn out to have an acceptable DOS value in the DL-EPR test (and resistant to IGC).

The DOS values reported in Table 3 for the two types of weldments show higher value for the HAZ and WFZ (1.4–4.2) as compared to the value for the SA material (0.43). The heat input and cooling rate of a welding technique would indirectly affect carbide precipitation in the microstructure of weldments. The heat input calculated for LB welding was about 15 times lower than the TIG welding in the present study. The HAZ and WFZ of LB weldments showed lower DOS values compared to that for TIG weldments due to lower heat input of the welding technique. The IGC generally takes place in chromium depletion zones around the carbide precipitates in the dendritic regions of weld [44, 45]. The decreased carbide as seen in LB weldments due to low heat input contributes to decreased DOS values. It has been found that the grain boundary Cr level is a sensitive function of the size and density of the carbides along the boundary and of the distance from the carbide itself [45]. The HAZ (0.7 mm) and WFZ (2 mm) width of LB weldment is also comparatively smaller than corresponding HAZ (2 mm) and WFZ (6 mm) of TIG weldment which is a reflection of lesser heat input of the LB welding technique. Thus LB welding has an advantage in avoiding sensitization in weldments as compared to TIG welding. Thus the LB weldments would show an increased resistance to IGC and IGSCC resistance in reactor environment. IGSCC of stainless steels and nickel base alloys has been reported from both BWRs and PWRs. Hence the increased IGC resistance for LB weldments as compared to TIG weldments for Alloy 600 can be primarily used for PWRs as well as BWRs.

Table 3: Measured DOS values from DL-EPR test for Alloy 600 TIG and LB weldments.

Alloy test solution	Base metal (%)	TIG weldment (%)		LB weldment (%)	
	SA	HAZ	WFZ	HAZ	WFZ
Alloy 600 0.01 M H_2SO_4 + 0.00002 M KSCN (deaerated) at RT	0.43 (±0.01)	1.77 (±0.08)	4.2 (±0.19)	1.40 (±0.07)	3.7 (±0.17)

4 Conclusions

The reactivation behavior of Alloy 600 in the welded condition showed that sensitization of the alloy depended on the heat input of the welding technique. The DL-EPR technique is shown to be a better technique for assessing the degree of sensitization and IGC susceptibility. The high carbon content and the type of carbide formed (Cr_7C_3) in Alloy 600 are shown to be the reason for formation of chromium depletion regions. The laser beam weldments showed lower DOS values (in HAZ and WFZ regions) as compared to that in TIG weldment due to the lower heat input and faster cooling rates resulting in lesser carbide precipitation and hence decreased chromium depletion. This results in an increased resistance to IGC.

Acknowledgments: The authors would like to acknowledge Dr. R. Tewari for his help in analyzing the TEM-SAD pattern.

Received: May 14, 2013. Accepted: June 30, 2013.

References

[1] D.J. Tillock, Selection of Nickel, Nickel-Copper, Nickel-Chromium and Nickel-Chromium-Iron Alloy, Welding, Brazing and Soldering, ASM Handbook, Vol. 6 (1993) 589.

[2] G.P. Airey, A.R. Vaia, and R.G. Aspden, Nucl. Tech. 55 (1981) 436–448.

[3] T.U. Martson and R.L. Jones, Proc. Fifth Int. Symp. on Environmental Degradation of Materials in Nuclear Power Systems – Water Reactors, American Nuclear Society, D. Cubicciotti, E.P. Simonen, and R. Gold (eds.), La Grange Park, Illinois (1991).

[4] R.W. Staehle, Proc. 5th Int. Steam Generator Conference, Canadian Nuclear Society, Toronto, Nov. 2006.

[5] BUGEY 2–3 NPP – Unit 3 – Vessel head – Penetration #54 – Examination of the segment bored from the head. MRP-EDF-CRDM07.

[6] C.M. Owens, T.P. Magee, and J.F. Hall, Failure analysis report TR-MCC-306, October 1993.

[7] BWXT Services, Inc., Failure analysis report 1140-015-99-75, February 2001.

[8] D.E. Whitaker, Nuclear Generation, Final Data Report for Metallurgy File #2749, January 2001.

[9] BWXT Service, Inc., Failure analysis report 1140-030-03-57:2, September 2003.

[10] R. Killian, R. Zimmer, and M. Widera, Proc. 13th Int. Conf. on Environmental Degradation of Materials in Nuclear Power Systems, Whistler, B.C., Canada, August 2007.

[11] R.L. Tapping, Y.C. Lu, and M.D. Pandey, Proc. 13th Int. Conf. on Environmental Degradation of Materials in Nuclear Power Systems, Whistler, British Columbia, August 2007.

[12] H. Coriou, L. Grall, C. Mahieu, and M. Pelas, Corrosion, 22 (1966) 280–287.

[13] R.B. Rebak and S. Szklarska-Smialowski, Corros. Sci., 38 (1996) 971

[14] J. Blanchet, H. Coriou, L. Grall, C. Mahieu, C. Otter, and G. Turluer, Proc. of the Stress Corrosion Cracking and Hydrogen Embrittlement of Iron Base Alloys, NACE, Houston, TX (1973).

[15] R. Kilian, N. Wieling, and L. Stieding, Werkst. und Korros., 42 (1991) 490–496.

[16] V. Kain and Y. Watanabe, J. Nuclear Materials, 302 (2002) 49–59.

[17] H.T. Lee and J.L. Wu, Corros. Sci., 51 (2009) 439–445.

[18] R. Kaul, S. Mahajan, V. Kain, P. Ganesh, K. Chandra, I. Samajdar, A.K. Nath, and R.C. Prasad, Corrosion, 64(10) (2008) 755–763.

[19] K. Chandra, V. Kain, and P. Ganesh, ASM J. of Mat. Engg. and Perf., 17(1) (2008) 115–122.

[20] J.D. Kim, C.J. Kim, and C.M. Chung, J. Mater. Process. Technol., 114 (2001) 51–56.

[21] T. Nagashima, A. Yokoyama, T. Akaba, Y. Nagura, O. Matsumoto, and T. Ishide, Weld. World, 34 (1994) 133–138.

[22] J.J. Kai, G.P. Yu, C.H. Tsai, M. Niliu, and S.C. Yao, Metall. Trans. A, 20A (1989) 2057.

[23] P.M. Scott, Corrosion Issues in Light Water Reactors: Stress Corrosion Cracking, D. Féron and J.M. Olive (eds.), Woodhead, England, (2007) 3–24.

[24] ASTM Annual Book of Standards A262 (2010), Standard Practices for Detecting Susceptibility to Intergranular Attack in Austenitic Stainless Steels.

[25] ASTM Annual Book of Standards G28-02 (2008), Standard Test Methods for detecting susceptibility to intergranular corrosion in wrought, nickel-rich, chromium bearing alloys.

[26] ASTM Annual Book of Standards G108-94 (2010), Standard Test Method for Electrochemical Reactivation (EPR) for Detecting Sensitization of AISI Type 304 and 304L Stainless Steels.

[27] C. Huang, Y. Chang, and S.C. Chen, Corros. Sci., 46 (2004) 1501–1513.

[28] ASTM Annual Book of Standards E1473-09, Standard Test Methods for chemical analysis of nickel, cobalt and high temperature alloys.

[29] Special Metals Corporation, “INCONEL alloy 600”, Publication Number SMC-027 (2004).

[30] V. Cihal, T. Shoji, V. Kain, Y. Watanabe, and R. Stefec, EPR – A Comprehensive Review, FRRI publication (2004) 152.

[31] P.W. Fuerschbach and D.O. MacCallum, Proc. 14th Int. Congress on the Applications of Lasers and Electro-Optics (ICALEO ’95), California, (1995) 493.

[32] P.W. Fuerschbach, Weld. J. 75 (1996) 24–34.

[33] D.R. Johns and F.R. Beckitt, Corros. Sci., 30(2/3) (1990) 223–237.

[34] G.J. Abraham, Ph.D Thesis from IIT Bombay, Mumbai, March 2012.

[35] A. Borello and A. Mignone, Br. Corros. J., 17(4) (1982) 176–183.

[36] I.I. Kornilov, Iron Alloys 3, Acad. Sci. USSR Press, M., (1956).

[37] M. Kowaka, H. Nagano, T. Kudo, Y. Okado, M. Yagi, O. Takaba, T. Yonezawa, and K. Arioka, Nucl. Technol., 55 (1981) 394–404.

[38] Y.S. Lim, H.P. Kim, J.H. Han, J.S. Kim, and H.S. Kwon, Corros. Sci., 43 (2001) 1321–1325.

[39] K. Stiller, J. Nilsson, and K. Norring, Metall. Mater. Trans. A, 27A (1996) 327–341.

[40] W.T. Tsai, M.J. Sheu, and J.T. Lee, Corros. Sci., 38 (1) (1996) 33–45.

[41] G.S. Was, H.H. Tischner, and R.M. Latanision, Metall. Mater. Trans. A, 12A (1981) 1397–1408.

[42] E.L. Hall and C.L. Briant, Metall. Mater.Trans. A, 16A (1985) 1225–1236.

[43] R.C. Scarberry, S.C. Pearman, and J.R. Crum, Corrosion, 32 (1976) 401–406.

[44] S.L. Jeng and H.T. Lee, Mater. Trans. JIM, 48 (2007) 1–9.

[45] E.L. Hall and C.L. Briant, Metall. Trans. A, 15A (1984) 793–811.